RESEARCH ARTICLE

EARTH SCIENCES

Increasingly severe thermal stresses on global photosynthesis using insights from observations of canopy temperature

Tianbo Pan[1], Hao Xu[1,2*], Chris Huntingford[3], Shuchang Tang[1], Kai Wang[1], Josep Peñuelas[4,5], Shilong Piao[1*]

[1] Sino-French Institute for Earth System Science, College of Urban and Environmental Sciences, Peking University, Beijing 100871, China.

[2] International Institute for Applied Systems Analysis, Laxenburg 2361, Austria

[3] UK Centre for Ecology and Hydrology, Wallingford OX10 8BB, UK

[4] CREAF, Catalonia, Barcelona 08193, Spain

[5] CSIC, Global Ecology Unit CREAF-CSIC-UAB, Barcelona 08193, Spain

*Corresponding author:

Shilong Piao (slpiao@pku.edu.cn), Hao Xu (xuhao@iiasa.ac.at)

Abstract

Temperatures could routinely exceed the optimal levels for photosynthesis as global warming intensifies, imposing thermal stress on the productivity of vegetation. We utilised satellite-derived canopy temperature and gross primary productivity (GPP) data from 2003 to 2024 to identify the ecosystem-level optimal canopy temperature (T_{opt}^{can}) for global photosynthesis and the extent of any thermal acclimation, which may offset warming impacts. Our findings indicated that across the globe, heat-induced restrictions on global photosynthesis are worsening, and areas subjected to thermal limitations have expanded by 1.7 billion hectares (57% increase) over the last 22 years. The number of days per year with high thermal suppression of photosynthesis during that period has increased sharply, averaging 28 days globally, and is especially high in tropical forests (117 days) and key agricultural regions (39 days). We demonstrate that vegetation acclimation to higher canopy temperature is partially mitigating emerging heat stress, but it is insufficient to keep up with the rate of global warming, with more than 90% of vegetated areas, and from locations across the globe, exhibiting partial acclimation. A key feature of our analysis is the use of canopy-level temperatures, which more accurately represent the actual temperatures that vegetation physiologically responds to, rather than previous research using air temperature. This difference accounts for our identified more rapidly intensifying vegetation response to warming than that estimated by other analyses. Overall, our canopy-level analysis reveals an escalating threat to global vegetation productivity and highlights the need for climate models to have refined land components, which often rely on air-temperature forcing and simplified acclimation schemes. Required are targeted ecosystem management strategies for adaptation to further global warming.

Keywords: canopy temperature, gross primary productivity, optimum temperature, thermal acclimation, thermal stress

Main Text

Photosynthesis, as a fundamental component of plant growth and the carbon cycle, provides food and fibre that are essential for ecosystems and society [1,2]. The rate of photosynthetic carbon sequestration in plants is highly sensitive to global warming across scales, from individual leaves to entire ecosystems [3–5]. The temperature response of photosynthesis typically follows a unimodal curve that first increases relatively slowly with temperature until it exceeds the optimum (T_{opt}) [6–8], after which the rate declines very rapidly. This substantial asymmetry implies that knowing T_{opt} is crucial, as should the temperature rise above it, then a strong suppression of photosynthesis will occur. Hence, insights into T_{opt} values provide vital information for assessing the margin of safety between current warming levels and the higher optimal temperature [9–12], or the extent to which thermal limits have been reached [13,14] under climate change. Heatwaves have become more frequent and widespread in recent decades, and in tandem with ongoing background climatic warming, this has caused many instances of observed severe suppression of vegetation productivity and even large-scale die-offs [15–17]. These rapidly escalating heatwaves and associated extreme temperature events underscore, in particular, the pressing need for a thorough data-led evaluation of the current state and changes in thermal limitation risk for global vegetation.

Field experiments and biochemical models suggest that plants can partially adapt to varying background temperature levels by self-regulation [6,18]. For example, tropical plants exhibit a higher T_{opt} than plants in temperate and boreal regions [8,19]. T_{opt} can also increase (i.e., acclimate) with rising temperature and the concentration of atmospheric carbon dioxide (CO_2), alleviating any potential negative impacts of human-induced global warming on photosynthesis [12,20]. However, considerable debate persists regarding whether global vegetation can fully acclimate to changes in temperature on a decadal scale, and if not, then what is the extent of partial acclimation that may occur [8,21,22]. Previous studies have primarily relied on space-for-time substitution to estimate rates of acclimation [8,12], which implicitly assume that vegetation thermal optima are in (or close to) equilibrium with the local climate (i.e., near-unity

tracking of warming). However, spatial variation in T_{opt} largely reflects long-term adaptation to the climate of origin, whereas temporal changes over recent decades are constrained by shorter-term physiological acclimation and ecological limits [23,24]. As a result, space-for-time approaches may overestimate the capacity of T_{opt} to track rapid contemporary warming. Furthermore, while leaf- and site-level studies provide critical physiological insights [25–28], ecosystem-scale assessments remain scarce. Few studies explicitly assess whether observed temporal adjustments in T_{opt} actually reduce exposure to supra-optimal heat stress. Taken together, these gaps reflect an insufficient understanding of the short-term thermal acclimation of ecosystem-scale T_{opt}, which in turn greatly impedes our ability to accurately quantify the capacity of vegetation to cope with a warming world.

Much of our knowledge of ecosystem-level T_{opt} arises from studies examining the response of photosynthesis to ambient air temperature (T_{air}) [8,12,21,22]. Although this approach yields valuable information, photosynthesis is more directly governed by the leaf temperature (T_{leaf}) [29] or canopy temperature (T_{can}). Substantial evidence shows that T_{can} can significantly differ from air temperature due to the influence of environmental controls (e.g., water stress and solar radiation), foliar traits, and canopy structure [28–33]. While transpirational cooling and microclimatic buffering can maintain T_{can} below or increase more slowly than T_{air} [34,35], intense solar radiation can conversely drive T_{can} above or warm faster ambient air temperatures [36,37]. These driving mechanisms often coexist, exhibiting complex spatial and temporal heterogeneity in the patterns of canopy temperature [36,38]. With the continuously expanding availability of canopy temperature observations from thermal cameras and satellites [13,31], we now have the opportunity to gain novel insights into the more physiologically relevant response of photosynthesis to temperature at the canopy scale.

Here, we used simultaneous satellite-derived observations of canopy temperature (T_{can}) and gross primary productivity (GPP) to investigate how photosynthesis has responded to changes in canopy thermal conditions over the last two decades (2003–2024) (see *Methods*). Although

the temperature response of photosynthesis is ultimately determined at the leaf scale, we emphasize that T_{can} used here represents an ecosystem-scale, spatially integrated radiometric signal of the vegetation canopy rather than the temperature of individual leaves or specific canopy layers. It serves as a robust proxy for the thermal environment experienced by vegetation and covaries closely with leaf temperature over broad spatio-temporal scales. Consistent with this, both canopy temperature and vegetation productivity in our study represent spatially and vertically integrated canopy- to ecosystem-scale signals rather than leaf-scale measurements.

Using the full record, we first characterized the global distribution of the optimal canopy temperature for ecosystem photosynthesis (T_{opt}^{can}) and explored its dependence on background climatic conditions. We then quantified local shifts in T_{opt}^{can} over the last 22 years to assess whether thermal acclimation has occurred. Finally, we evaluated changes in the magnitude and range of thermal conditions experienced by global vegetation, with a particular focus on the extent and frequency of supra-optimal heat stress and on whether acclimation has kept pace sufficiently to constrain such stress. To contextualize our findings, we compared our results against traditional T_{air}-based assessments in our analysis to investigate how reliance on T_{air} may have influenced previous estimates [8,12,21,22] relative to the actual thermal conditions experienced by plant canopies. The robustness of our results was further verified using three alternative GPP proxies: the near-infrared reflectance of vegetation (NIR_V) [39], its photosynthetically active radiance-multiplied product (NIR_VP) [40], and the contiguous solar-induced chlorophyll fluorescence (CSIF) [41]. In addition, we independently evaluated the satellite-derived T_{can} against site-scale aerodynamic canopy temperature estimates derived from eddy-covariance observations. By integrating a physiologically grounded canopy-temperature framework, high-resolution (1-km) observations, and extended temporal coverage, our study aims to advance the previous research [8,12,21,22], providing an explicit assessment of how vegetation thermal exposure and acclimation capacity are evolving in a warming world.

Results

Spatial distribution of T_{opt}^{can}

We identified the global pattern of T_{opt}^{can} for photosynthesis by using simultaneous satellite observations of canopy temperature and GPP data from 2003 to 2024 inclusive (see *Methods*). The average T_{opt}^{can} across all global vegetated areas was estimated to be 30±6°C (mean ± 1 standard deviation), with 98% of the areas falling within the range of 20–50°C (Fig. 1a, b). T_{opt}^{can} exhibited substantial geographical heterogeneity in its spatial distribution, as shown in Fig. 1a. Along latitudinal gradients, higher values of T_{opt}^{can} were found in tropical regions (33±4°C) compared to polar regions (25±4°C), which are generally warmer locations due to more intense solar radiation. Arid regions such as the Sahel, the Somali Peninsula, the central United States of America, central Asia, and northern Australia had especially high T_{opt}^{can} values nearing 50°C, likely due to the additional effect of limited water availability. In addition, lower values of T_{opt}^{can} close to 20°C were observed in high-altitude regions like the Tibetan Plateau and the Andes in Chile. We also estimated the global optimal air temperature (T_{opt}^{air}) for photosynthesis using air temperature from the ECMWF Reanalysis v5 (ERA5-Land) product (Fig. S1a). T_{opt}^{can} and T_{opt}^{air} exhibited similar spatial patterns, but T_{opt}^{air} (25±5°C) was substantially lower than T_{opt}^{can} (Fig. 1b and Fig. S1a). This discrepancy occurred because the cooling effect of foliar transpiration during daytime photosynthesis, particularly under strong midday sunlight, is insufficient to counteract radiative heating [35,36], thereby leading to canopy temperatures that exceed the ambient air temperature. This difference was especially pronounced in arid regions (Fig. S1b), where it could exceed 15°C due to further restrictions on transpiration.

We then analysed how optimal temperatures depend on background precipitation levels and temperature forcings. Hence, in Figs. 1c, d we present T_{opt}^{can} and T_{opt}^{air} as functions of the climatic space defined by both mean growing-season daily maximum air temperature (T_{gs}^{air}) and mean annual precipitation (MAP). Both T_{opt}^{can} and T_{opt}^{air} increased with background temperature around the globe, consistent with both previous studies attributing this relationship to evolutionary adaptation [6–8,42] and features of Fig. 1a. The spatial sensitivities of T_{opt}^{can} and T_{opt}^{air} to T_{gs}^{air} were

positive but less than unity for most precipitation bins (right-hand panels of Fig. 1c, d), suggesting that spatial gradients of T_{opt}^{can} generally follow, but do not fully keep pace with the increases in background temperature. This difference may be due to hydraulic and phenological limitations or caused by lower interannual variability in warmer regions [43]. The sensitivities of T_{opt}^{can} and T_{opt}^{air} to background temperature were robust (Fig. S2), regardless of how background temperature was defined and whether employing daily maximum instead of daily average temperature or using annual instead of growing-season data.

Notable, however, was that T_{opt}^{can} consistently exhibits negative (i.e. decreasing) sensitivity to increasing background precipitation across most temperature ranges (Fig. 1c). This suggests that vegetation in drier environments can tolerate high foliar temperature extremes by having more raised T_{opt}^{can} values (as also reflected geographically in higher T_{opt}^{can} values; Fig. 1a). Plants in arid regions often close their stomata, or reduce stomatal density, to minimise the loss of water, but this also results in reduced transpirational cooling and consequently higher foliar surface temperatures [10,44,45]. Given this trade-off, plants tend to adapt by allowing higher foliar temperatures rather than potentially dying from the loss of water, and this may also explain the higher T_{opt}^{can} values in such locations. Our findings in Fig. 1a and 1c suggest the capability of plants to enhance their heat tolerance by physiological and morphological adjustments, or by altering community composition, such as by increasing the proportion of heat-tolerant C_4 plants [46]. Knowledge of canopy temperature, therefore, effectively integrates the effects of both ambient air temperature and water stress, to give a reliable estimate of optimal temperature, T_{opt}, as a function of both these climatological drivers. This negative sensitivity of T_{opt}^{can} to MAP remains consistent across different background temperatures (Figs. S2 and S3). However, T_{opt}^{air} depended only weakly on spatial variations in precipitation, with sensitivities close to or slightly above zero across most temperature bins (Fig. 1d). This finding suggests that air temperature does not capture the adaptation of vegetation to water stress, likely due to its poor representation of the physiological and structural responses of vegetation to environmental change [31,38]. These errors matter, as in a changing climate that is altering both

temperature and aridity levels, it is important to avoid compensating errors appearing in any dependencies of calibrated parameters of vegetation models, such as T_{opt}. These findings were also consistently reproduced when using alternative GPP proxies (NIR_V, NIR_VP and CSIF; Figs. S4-S6).

Thermal acclimation of T_{opt}^{can}

The optimal temperature for global photosynthesis is not static, and this holds particular importance in the context of rapid climate warming caused by human burning of fossil fuels. We found that the T_{opt}^{can} value for vegetation productivity increased significantly from 2003 to 2024 at both regional and global scales. The globally average value of T_{opt}^{can} increased by approximately 0.076℃ y^{-1} over the last 22 years (Fig. 2b). Regionally, T_{opt}^{can} tended to increase with statistical significance (i.e. with a regression fit of P-value<0.05) in 19% of vegetated areas worldwide, while it decreased significantly in only about 0.01% of the vegetated areas (Fig. 2a). Optimal temperatures exhibited a more widespread significant increase in tropical regions (0.083℃ y^{-1}) and so at a rate higher than the global average. In some high-latitude areas and arid regions, the rate of increase was even more rapid, reaching up to 0.4℃ y^{-1}, though substantial spatial heterogeneity was observed in both instances. In comparison, the global increase in projected T_{opt} when derived from air temperature was about 0.042℃ y^{-1}, suggesting, possibly incorrectly, markedly slower changes in canopy temperatures (Fig. 2a and Fig. S7).

A key question is whether the observed changes in T_{opt} have tracked global warming and hence demonstrated a capacity to acclimate thermally to anthropogenic climate change. To assess this, we quantified the magnitude of thermal acclimation for each vegetation grid as the ratio $\partial T_{opt}^{can} / \partial T_{max}^{can}$, derived from the regression coefficient between T_{opt}^{can} and T_{max}^{can} over the 22-year study period (Fig. 2c). Globally, we find that thermal acclimation is overwhelmingly partial. Vegetation exhibited an average acclimation magnitude of 0.37 °C per 1 °C, with over 90% of vegetated areas falling below unity (the 1:1 tracking benchmark). This empirical evidence at the ecosystem scale confirms that vegetation has only partially kept pace with rising heat stress,

a finding remarkably consistent with established leaf-level observations [24–27]. Spatially, thermal acclimation was strongest and most significant in high-latitude regions (Fig. 2c, d), likely driven by large interannual temperature variability [22], warming-induced stimulation of nitrogen mineralization [48], and rapid shifts in species composition toward more productive functional groups [49]. This suggests that vegetation in these regions may be better able to cope with intensifying heat stress. Tropical rainforests also exhibited spatially widespread significant acclimation (Fig. 2c); however it failed to fully track the imposed climate change. Because ambient temperatures in these biomes are already approaching critical physiological thresholds [13], such partial adjustment provides only limited protection against future warming. In contrast, most other regions showed weak or insignificant acclimation. Such limited responses could arise from insufficient temporal changes in canopy temperature to trigger acclimation [8] or from inherent physiological and ecological constraints that prevent thermal adjustment on decadal timescales. Moreover, species with broad photosynthetic thermal response curves may not need to shift T_{opt} [50], as moderate temperature changes do not substantially suppress their photosynthetic capacity. Finally, thermal acclimation estimated from air temperature exhibited similar spatial patterns, confirming the overall incomplete acclimation of vegetation to warming (Fig. S8). However, magnitudes based on air temperature were generally lower in tropical, arid, and temperate regions, but higher at high latitudes, reflecting regional biases when using air temperature to assess acclimation. These findings remained highly consistent across multiple GPP proxies (NIR_V, NIR_VP, and CSIF; Figs. S9-S11), confirming the robustness of our finding that global vegetation acclimation is insufficient to keep pace with a warming climate.

Expansion of thermally limited area

To move beyond mapping T_{opt}^{can} patterns and trends in previous studies [8, 21], we explicitly quantified supra-optimal heat stress exposure across global vegetation. We analysed the difference between T_{opt}^{can} and T_{gs}^{can} from the years 2003 to 2024 and across global vegetation, to determine whether high temperatures have become a limiting factor for canopy photosynthesis. Given the strong nonlinearity at high temperatures in the photosynthetic response, we are

particularly interested in whether $T_{gs}^{can} > T_{opt}^{can}$. Our findings illustrate that the multi-year mean T_{gs}^{can} under current mean-decadal climatic conditions is substantially higher than the value of T_{opt}^{can} in arid and semi-arid regions such as Central America, the southeastern Amazon Basin, African savannas, the Somali Peninsula, India, Australia, and central Asia (Fig. 3a, b). The suggestion is that photosynthesis in these areas has been persistently constrained by thermal stresses (Fig. 3a, b). And the optimal temperature in the three major regions with tropical rainforest was already slightly lower (1.0±2.0°C) than the average temperature during the growing season (Fig. 3a), leaving no remaining safety margin for photosynthesis and posing an even greater risk especially if any acclimation does not keep pace with future warming. In contrast, mid- to high-latitude regions in both hemispheres still retained a large safety margin, where warming could continue to enhance photosynthesis (Fig. 3a, b). The pattern of differences between optimal and average air temperature was similar to that when using canopy temperatures in calculations (Fig. 12), although the level of thermal limitation was less pronounced (Fig. 3b).

The areas subjected to normalised thermal limitation have gradually expanded over the last 22 years as warming has intensified (red overlay in Fig. 3a, with the definition in the caption; see also Fig. 3c). Globally, areas where the average growing-season canopy temperature (T_{gs}^{can}) exceeded T_{opt}^{can} have increased from approximately 3.0 billion to 4.7 billion hectares during that period and should there be no acclimation (and thus an annual rate of increase of 84 million hectares Mha y^{-1}; Fig. 3c, red curve). This expansion has notably accelerated in the last decade (Fig. 3c). As might be expected, most of the expansion occurred at the edges of existing thermally limited areas, with widespread expansion in the southern Amazon Basin, the African Sahel and southern Africa, Madagascar, and Mexico. Additionally, despite the significant capability of T_{opt}^{can} to acclimate to recent background warming in many locations (Fig. 2), this physiological adjustment has only marginally decelerated the expansion of these heat-limited areas over the last two decades. Specifically, acclimation has slowed the rate of expansion from 84 to 67Mha y^{-1} by adjusting T_{opt}^{can}. The rate of expansion would still exceed estimates based on air temperature (38Mha y^{-1} without acclimation and 32Mha y^{-1} with acclimation). Comparable

273 results were obtained when using alternative GPP proxies (Figs. S13-S15).

274

275 **The increasing frequency of thermal limitations**

276 In addition to our derivation above of the expansion of thermally limited areas, we also
277 considered temporal variations for particular fixed locations. Specifically, we analysed the
278 changes in the number of days within the growing season each year when canopy temperature
279 exceeded T_{opt} levels, thereby impacting vegetation growth and photosynthesis. It is noted that
280 there may not be a simple one-to-one correspondence between rates of background warming
281 and increases in extreme events, caused by a straightforward shift in the distribution of daily
282 temperatures. Instead, for some locations, very high-temperature events have recently
283 accelerated relative to general warming changes [52]. Although the number of extremely high-
284 temperature days in our study was low in regions such as tropical rainforests and high-latitude
285 regions around the globe (Fig. S16), high-temperature events are increasing in their occurrence
286 under recent warming. The global average number of days when heat could potentially suppress
287 productivity for vegetation has increased at a rate of 1.26 d y^{-1} from 2003 to 2024 although this
288 statistic is derived without considering thermal acclimation (Fig. 4a). During this period, 64%
289 of global vegetated areas experienced a statistically significant increase in the number of high-
290 temperature events, with rates from 0.38 to 6.92 d y^{-1}, corresponding to the 95% confidence
291 interval (dot markers and positive values; Fig. 4a).

292

293 Tropical forests, in particular, have experienced a substantial and widespread increase in the
294 number of high-temperature limited days (Fig. 4f-h), especially when not accounting for
295 acclimation. This finding suggests that global warming has the potential to cause much more
296 routine overriding of safe thermal margins in those locations. In the Amazon rainforest (Fig.
297 4f), high-temperature limited days have increased by nearly 120 days over the last 22 years. In
298 earlier periods, these high-temperature episodes often coincided with major El Niño events,
299 such as in years 2005, 2010, and 2015/2016. The rate of increase in canopy temperature over
300 the last five years, however, has far outpaced the rate in previous years, and this cannot be

linked to natural variation via El Niño alone. The frequency of possibly damaging high-temperature events also increased substantially in the Congo rainforest (Fig. 4g) and forests in southeastern Asia (Fig. 4h), particularly over the last decade. The vegetation thermal-suppression period has increased by 0.8–3.1d yr^{-1} in major agricultural regions such as eastern Europe (Fig. 4b), Indo-China Peninsula (Fig. 4c), the North China Plain (Fig. 4e) as well as savannas in African and the southeastern Amazon Basin (Fig. S17), and boreal forests in central Siberia (Fig. 4d). Other high-latitude boreal forests, however, have not changed significantly, indicating that they still have a considerable margin of safety for future warming (Fig. 4a) and even in the absence of thermal acclimation. These geographical differences may again reflect that for locations with higher interannual variability in temperature (e.g., more poleward), background warming may be less impactful. It is noted that the number of high-temperature limited days based on air temperature was comparable to the number based on canopy temperature (Figs. S16 and S18a), but its trends were much weaker (Fig. 4 and Fig. S18b).

Our data-led investigations have revealed the potential of vegetation to acclimate by quantifying the time-evolving values of T_{opt}^{can}. Such knowledge of T_{opt}^{can} changes allows us to determine, by region, the extent to which acclimation capability mitigates the increases in temperatures that would otherwise reduce vegetation productivity. However, we found that thermal acclimation played only a limited role in alleviating heat stress (Fig. S19). Even after accounting for acclimation, 58% of global vegetated areas still experience a significant increase in thermal events (only slightly lower than 64% without acclimation). In tropical rainforests, widespread significant acclimation provides notable mitigation, with the annual rate reduction approaching 2 d yr^{-1} (Fig. 4f-h). Nevertheless, despite this buffering effect, the overall frequency of thermal limitations continues to rise rapidly, indicating that even substantial physiological adjustments are being outpaced by the rate of warming in these critical ecosystems. In contrast, across many other regions, including major agricultural areas, acclimation has only a slightly marginal rate of increase in days of vegetation productivity suppression (Fig. 4b-e). Together, these findings imply that the inherent adaptive capacity of

vegetation in these areas was insufficient, leaving ecosystems still at considerable risk under the current pace of human-driven warming. Additionally, these conclusions are highly robust across multiple productivity proxies (Figs. S20-S22).

Discussion and Conclusions

Our data-driven findings highlight the escalating threat of thermal stress on vegetation due to human-induced climate change. Such stresses occur particularly when temperatures exceed the photosynthetic threshold of T_{opt}^{can}, as above this value, productivity is rapidly suppressed. Under the initial assumption of invariance in T_{opt}^{can}, areas experiencing potential thermal limitations have expanded substantially, from 3.0 billion to a more recent coverage of 4.7 billion ha, comparable to the size of two Amazon rainforests (Fig. 3). Simultaneously, the frequency of thermally limiting events (i.e. when canopy temperature exceeds T_{opt}^{can}) has risen sharply, particularly in tropical forests and many agricultural regions (Fig. 4). In particular, the rate of intensification of heat stress over the recent five years period of 2018–2024 has far exceeded previous records (Figs. 3 and 4), consistent with the increasing observed frequency and scope of extreme heatwaves in recent years [5,15,16]. Continuation of these trends would pose a serious threat to the global terrestrial carbon sink, carbon-neutral targets in the future, and the overall health of land ecosystems or the ability to grow crops [53].

We mainly base our assessment of changes in thermal stress on satellite-derived canopy temperature, as this represents more accurately the thermal regimes experienced by vegetation [30,32] (Fig. 1). Our analysis reveals a more rapidly escalating heat stress than the calculated changes based on air temperatures (Figs. 3 and 4). This finding suggests that previous evaluations, instead of undertaking calculations with air temperatures only [8,14,54], while making valuable contributions to understanding, may have underestimated the thermal risks to vegetation. Recent studies increasingly showed that the rate of warming under climate change at the top of a canopy may outpace the increase in air temperature due to changes in the physiological responses of the vegetation and radiation balance of the canopy [13,36].

Additional environmental stresses, such as water scarcity and reduced wind speeds, may further accelerate increases in canopy temperature [30,55,56]. These differences account for our larger increasing trends in exposure to high temperatures when based on canopy temperature, to which vegetation responses are more tightly linked.

By extending our analyses to include temporal variation in T_{opt}^{can}, we identified a thermal acclimation capability for many locations. Again, we suggest that our findings derived from canopy temperature, rather than air temperature, are likely to be more accurate, due to their ability to capture more directly the vegetation responses to environmental changes [30,32]. We found that over the past 22 years, the optimal canopy temperature has increased significantly in approximately 19% of global vegetated regions, and with these rises distributed across the planet (Fig. 2b). The primary drivers of this increase include elevated CO_2 concentrations [10,57], physiological and morphological adjustments in plants [7,43,58], and shifts in community composition favouring heat-tolerant species [59–61]. In photosynthesis models, elevated CO_2 concentrations can interact with a temperature response function such that the combined response simulates increases in maximum T_{opt}^{can}. Alternatively, model parameters that might have previously been considered invariant may themselves adjust to raised temperatures (i.e., acclimate), a concept tested at a range of locations using eddy covariance measurements [62]. Our integrated framework merges independent strands of Earth Observation data to provide a globally complete assessment of ecosystem thermal acclimation. This advancement is of significant utility for the calibration and refinement of the land-surface components within Earth System Models (ESMs), which currently struggle to represent dynamic physiological adjustments. Moving beyond previous assessments that focused solely on the existence of acclimation [21,22], we evaluate the extent to which these physiological shifts actually mitigate intensifying thermal stress.

Our findings of thermal acclimation suggest that vegetation changes have slowed the rate of expansion and the increase in frequency of thermal suppression of vegetation in many locations

(Figs. 3 and 4), thus mitigating adverse warming impacts on photosynthesis and the carbon cycle. This regulatory capacity of vegetation, however, is limited and cannot fully negate the detrimental trends associated with warming. Regions with intensified thermal limitations and limited capacity to acclimate, and so having substantial rises in thermal stress (e.g., location of major agricultural areas in Figure 4), should be prioritised for greater attention and potentially specific targeted land management plants in the future. In addition to T_{opt}, recent evidence [63] suggests that the breadth of the photosynthetic temperature-response curve also significantly influences how vegetation responds to warming, which represents an important complementary dimension of thermal acclimation that warrants systematic investigation in future research.

While satellite-derived observations offer more physiologically relevant insights than air temperature [13,32], current thermal products primarily sample the radiometric temperature of the upper canopy and therefore cannot fully resolve thermal variation throughout the entire canopy profile [29]. Although the upper canopy accounts for the dominant proportion of total canopy photosynthesis [64], sub-canopy layers also contribute to productivity by utilizing diffuse and scattered light [65]. Site-specific research has shown, as expected, that the top of a canopy is exposed to the highest levels of solar radiation [64], whereas sub-canopy leaves are mostly shielded by the "parasol effect" [66], creating microclimate buffering [35] with the potential to lower leaf temperature. The magnitude of these effects within canopies may vary across forest types and climatic zones, yielding vegetation responses to climate change that are more complex than those at the top of the canopy alone [64]. Hence, our main caveat is that while the approach presented here does provide robust information on the likely overall response of vegetation to thermal stress, it may be insufficient to fully characterise the response of the full vertical temperature profile or the thermal response of every canopy stratum in a warming world [29,66]. Further measurements into vertical foliar temperature profiles across diverse biomes are essential to bridge the gap between satellite measurements and the metabolic response of the entire canopy [66].

In addition, although we applied strict quality control at 1-km resolution to preferentially retain vegetation-dominated pixels, satellite-derived T_{can} may still be affected by soil background, mixed pixels, and vegetation clumping, particularly in sparsely vegetated ecosystems such as savannas. These effects likely contribute to the small but systematic deviations (Fig. S23) between satellite-derived and eddy-covariance (EC)-based T_{can} observed in some sparse ecosystems. Encouragingly, validation against site-scale aerodynamic canopy temperature estimates derived from EC observations showed generally good agreement (Figs. S24 and S25), supporting the use of satellite-derived T_{can} as a meaningful proxy for ecosystem-scale canopy thermal conditions. Future work could further reduce these uncertainties by combining higher-resolution thermal observations with improved methods to separate canopy and soil thermal signals and to better resolve within-canopy temperature gradients.

Another critical frontier is the explicit incorporation of leaf temperature (T_{leaf}). While our canopy-based framework represents vegetation thermal conditions more accurately than air temperature [30,32], T_{leaf} remains the most physiologically direct driver of photosynthesis. Recent evidence indicates that the divergence between T_{can} and T_{leaf} can be substantial in certain ecosystems [28], implying that canopy-integrated estimates may represent a conservative baseline for leaf-level heat stress. However, global assessments are currently hindered by the scarcity of long-term T_{leaf} observations [28,67,68] and the fact that most ESMs do not yet provide standardized diagnostics for both T_{can} and T_{leaf}. Consequently, our analysis establishes a necessary canopy-scale benchmark, providing a foundation upon which future studies can build as sophisticated land-surface representations and comprehensive T_{leaf} monitoring networks become available.

Our study presents a novel, observation-led assessment of the recent historical response of photosynthesis to temperature and changes in thermal limitations, providing valuable guidance for ecosystem management in response to human-induced global warming. By capitalizing on simultaneous satellite measurements of canopy temperature and vegetation productivity, our

analysis achieves nearly global coverage, capturing the heterogeneous ways ecosystems respond to heat stress. As climate warming intensifies, the challenges posed by thermal limitations on vegetation will become more acute, requiring models that can accurately simulate these impacts to inform societal adaptation. Despite the incorporation of nonlinear temperature-productivity responses, current global vegetation models rely primarily on air temperature [69,70] or utilize overly simplistic representations of canopy temperature [71] as the thermal forcing, which limits their fidelity in simulating actual photosynthetic performance. Furthermore, mechanistic representations of thermal acclimation are frequently omitted or highly simplified [72,73], with existing parameterizations often constrained by air temperature forcing rather than the more physiologically relevant leaf or canopy temperature. A significant hurdle for the modelling community is that T_{can} is not yet a standardised diagnostic in most ESMs, which precludes robust multi-model comparisons of thermal optima. Our analysis directly addresses these gaps, providing a blueprint for using satellite-derived metrics to constrain advanced land-surface model configurations. Moving forward, integrating these satellite insights with in-situ data on within-canopy temperature profiles will be essential to refining our predictive capacity and ensuring the resilience of the global carbon sink.

Methods

Canopy temperature

We derive global canopy temperature (T_{can}) from the MODIS MYD21A1D land-surface temperature product at 1-km daily resolution for 2003-2024 [74]. Because land-surface temperature approximates T_{can} in densely vegetated and homogeneous pixels, we retained vegetation-dominated pixels as canopy signals after excluding non-vegetated and mixed pixels. Specifically, we used the maximum–minimum apparent emissivity difference threshold (MMD < 0.03) to reduce mixed-pixel and soil-background contamination [13,75] together with an annual mean NDVI > 0.1 mask to remove water bodies and sparsely vegetated areas [8,76]. The Aqua overpass time, around 13:30 local time, is close to the timing of peak daytime canopy temperature, allowing T_{can} to represent maximum thermal exposure. Missing daily values caused by cloud contamination or retrieval errors were gap-filled using a 10-day moving average and, where necessary, long-term means; years and grid cells with excessive missing data were excluded. Satellite-based T_{can} was independently evaluated against canopy temperature estimated from eddy-covariance observations using an aerodynamic resistance approach [77,78], showing robust agreement across temporal aggregation scales (Figs. S23-S25).

Gross primary productivity and climate data

Gross primary productivity (GPP), used as the primary indicator of ecosystem photosynthesis, was obtained from the MODIS MYD17A2HGP v6.1 product at 500-m and 8-day resolution [79]. We retained only good-quality and positive GPP values, then aggregated them to 1 km using area-weighted averaging to match the T_{can} dataset. The same MMD and NDVI filters were applied to ensure consistency between GPP and T_{can} observations. Growing-season months were derived from GIMMS leaf-area-index phenology and refined by excluding frozen periods [80]. To evaluate robustness, we further used three independent satellite-based proxies of photosynthetic activity: near-infrared reflectance of vegetation (NIRv) [39], NIRv multiplied by photosynthetically active radiation (NIRvP) [40], and contiguous solar-induced chlorophyll

fluorescence (CSIF) [41]. Climate variables included daily maximum air temperature from ERA5-Land [81], precipitation from the Global Precipitation Climatology Project (GPCP) [82], and independent validation using Climatic Research Unit and Japanese Reanalysis (CRUJRA) [83,84] (Fig. S26). Daily maximum air temperature was emphasized because peak daytime heat is most directly linked to thermal limitation of photosynthesis.

Optimal temperature for photosynthesis

The photosynthetic optimal temperature (T_{opt}) was estimated from the response of GPP to canopy or air temperature, with NIR_V, NIR_VP, and CSIF used for validation. For each 0.25° window, all native-resolution (e.g., 1-km) pixels and time steps were pooled to derive a single T_{opt} value, thereby retaining sub-grid variability while improving statistical robustness. Daily T_{can} was first averaged to the 8-day resolution of GPP. GPP observations were then grouped into dynamic temperature bins, with bin widths adjusted according to local temperature variability. Within each bin, the median of the five highest GPP values was used to represent near-unconstrained photosynthetic performance, minimizing the influence of other limiting factors such as cloudiness, radiation limitation, or drought. A running average across three adjacent bins was then applied, and T_{opt} was identified as the temperature corresponding to the maximum of the smoothed response curve. T_{opt} was estimated over the full 2003–2024 period for spatial analyses and annually to assess temporal shifts and thermal acclimation. Sensitivity tests using top-three, top-seven, and 90th-percentile [8] approaches yielded consistent results (Figs. S27 and S28).

Thermal acclimation

Thermal acclimation was defined as the temporal adjustment of T_{opt} to interannual variation in heat exposure [22]. For each grid, we regressed annual T_{opt} against annual maximum temperature (T_{max}) over the 22-year record, with the slope $\partial T_{opt}/\partial T_{max}$ representing the magnitude of acclimation. T_{max} was used because it better captures exposure to high-temperature conditions that constrain photosynthesis than growing-season mean temperature.

Grid cells without a significant T_{opt}-T_{max} relationship (P-value ≥ 0.05) were considered to lack detectable thermal acclimation and were assigned a fixed long-term T_{opt}. Where significant acclimation was detected, annual T_{opt} was dynamically adjusted according to the local T_{opt}-T_{max} relationship, isolates the temperature-driven component of T_{opt} variation from other confounding influences.

Supra-optimal thermal stress

We assessed supra-optimal thermal stress from both the extent and frequency of temperatures exceeding T_{opt}. The spatial extent of thermal limitation was defined as the area where growing-season mean temperature T_{gs} exceeded T_{opt}. Negative values of T_{gs}-T_{opt} indicated a remaining thermal safety margin, whereas positive values indicated that vegetation was already operating above its photosynthetic optimum and experiencing thermal suppression. We further calculated the annual number of days when daily maximum temperature exceeded T_{opt}, using both fixed and acclimation-adjusted T_{opt} values. Temporal trends in these heat-stress days were estimated using least-squares linear regression globally and across key carbon-sink and food-producing regions. Further details on datasets, preprocessing procedures, validation methods, T_{opt} estimation, thermal acclimation, and thermal-risk assessment are provided in the *Supplementary Information*.

Author contributions

S.P. and H.X. conceived the idea and designed the research. T.P. and H.X. performed the analysis and prepared the figures. T.P., H.X., C.H., and J.P. drafted the paper. S.T, K.W., and S.P. commented on the manuscript. All authors contributed to the interpretation of the results and revised the text.

Acknowledgements

This study was supported by the Second Tibetan Plateau Scientific Expedition and Research (STEP) program (2024QZKK0301) and the National Natural Science Foundation of China (42588201). The analysis and calculations were supported by High-performance Computing Platform of Peking University.

Data availability

All observational and reanalysis datasets used in this study are publicly available. MODIS data products (including LST, GPP, NIR_T, and NDVI) can be obtained from NASA's Land Processes Distributed Active Archive Center (LP DAAC: https://lpdaac.usgs.gov). The FLUXNET2015 dataset used for validation is available at https://fluxnet.org/data/fluxnet2015-dataset/. The incident photosynthetically active radiation (PAR) data from the Global Land Surface Satellite (GLASS) are available at https://www.glass.hku.hk/. The ERA5-Land reanalysis data and the GPCP v2.3 monthly precipitation product are accessible through the Copernicus Climate Change Service (C3S) Climate Data Store (https://cds.climate.copernicus.eu). The CRU-JRA reanalysis products are accessible via the CEDA Archive website (https://archive.ceda.ac.uk). The CSIF dataset can be accessed through Figshare (https://doi.org/10.6084/m9.figshare.6387494). The canopy temperature dataset and primary results generated in this study are archived on Figshare: https://figshare.com/s/719ca88d19f31a739e4b.

Code availability

All computer codes used for processing and analysing the data are available through Figshare: https://figshare.com/s/719ca88d19f31a739e4b.

Author contributions

The authors declare no competing interests.

References

1. Haberl H, Erb KH, Gaube V *et al.* Quantifying and mapping the human appropriation of net primary production in earth's terrestrial ecosystems. *Proc Natl Acad Sci USA* 2007; **104**: 12942–12947.
2. Piao S, Wang X, Park T *et al.* Characteristics, drivers and feedbacks of global greening. *Nat Rev Earth Environ* 2019; **1**: 14–27.
3. Dusenge ME, Duarte AG, Way DA. Plant carbon metabolism and climate change: elevated CO_2 and temperature impacts on photosynthesis, photorespiration and respiration. *New Phytol* 2019; **221**: 32–49.
4. Tiwari R, Gloor E, da Cruz WJA *et al*. Photosynthetic quantum efficiency in south-eastern Amazonian trees may be already affected by climate change. *Plant Cell Environ* 2021; **44**: 2428–2439.
5. Wolf S, Paul-Limoges E. Drought and heat reduce forest carbon uptake. *Nat Commun* 2023; **14**: 6217.
6. Berry J, Bjorkman O. Photosynthetic response and adaptation to temperature in higher plants. *Annu Rev Plant Physiol* 1980; **31**: 491–543.
7. Niu S, Luo Y, Fei S *et al.* Thermal optimality of net ecosystem exchange of carbon dioxide and underlying mechanisms. *New Phytol* 2012; **194**: 775–783.
8. Huang M, Piao S, Ciais P *et al.* Air temperature optima of vegetation productivity across global biomes. *Nat Ecol Evol* 2019; **3**: 772–779.
9. Duffy KA, Schwalm CR, Arcus VL *et al.* How close are we to the temperature tipping point of the terrestrial biosphere? *Sci Adv* 2021; **7**: eaay1052.
10. Lloyd J, Farquhar GD. Effects of rising temperatures and [CO_2] on the physiology of tropical forest trees. *Phil Trans R Soc B* 2008; **363**: 1811–1817.
11. Way D A. Just the right temperature. *Nat Ecol Evol* 2019; **3**: 718–719.
12. Chen A, Huang L, Liu Q *et al*. Optimal temperature of vegetation productivity and its linkage with climate and elevation on the Tibetan Plateau. *Glob Change Biol* 2021; **27**: 1942–1951.
13. Doughty CE, Keany JM, Weibe BC *et al.* Tropical forests are approaching critical temperature thresholds. *Nature* 2023; **621**: 105–111.
14. Nölte A, Yousefpour R, Cifuentes-Jara M *et al*. Sharp decline in future productivity of tropical reforestation above 29°C mean annual temperature. *Sci Adv* 2023; **9**: eadg9175.
15. Freychet N, Hegerl G, Mitchell D *et al*. Future changes in the frequency of temperature extremes may be underestimated in tropical and subtropical regions. *Commun Earth Environ* 2021; **2**: 28.
16. Wang J, Yan Z. Rapid rises in the magnitude and risk of extreme regional heat wave events in China. *Weather Clim Extrem* 2021; **34**: 100379.
17. Anderegg WRL, Kane JM, Anderegg LDL. Consequences of widespread tree mortality triggered by drought and temperature stress. *Nat Clim Change* 2013; **3**: 30–36.
18. Smith NG, Dukes JS. Plant respiration and photosynthesis in global-scale models: Incorporating acclimation to temperature and CO_2. *Glob Change Biol* 2013; **19**: 45–63.
19. Mau A, Reed S, Wood T *et al.* Temperate and Tropical Forest Canopies are Already Functioning beyond Their Thermal Thresholds for Photosynthesis. *Forests* 2018; **9**: 47.

20. Bennett AC, Arndt SK, Bennett LT *et al.* Thermal optima of gross primary productivity are closely aligned with mean air temperatures across Australian wooded ecosystems. *Glob Change Biol* 2021; **27**: 4727–4744.
21. Fang Z, Zhang W, Wang L *et al*. Global increase in the optimal temperature for the productivity of terrestrial ecosystems. *Commun Earth Environ* 2024; **5**: 466.
22. Wang Y, Sarmah S, Singha M *et al*. Increasing optimum temperature of vegetation activity over the past four decades. *Earth Future* 2024; **12**: e2024EF004489.
23. Wang B, Chen W, Tian D *et al.* Dryness limits vegetation pace to cope with temperature change in warm regions. *Glob Change Biol* 2023; **29**: 4750–4757.
24. Kumarathunge DP, Medlyn BE, Drake JE *et al.* Acclimation and adaptation components of the temperature dependence of plant photosynthesis at the global scale. *New Phytol* 2019; **222**: 768–784.
25. Way DA, Yamori W. Thermal acclimation of photosynthesis: on the importance of adjusting our definitions and accounting for thermal acclimation of respiration. *Photosynth Res* 2014; **119**: 89–100.
26. Slot M, Winter K. Photosynthetic acclimation to warming in tropical forest tree seedlings. *J Exp Bot* 2017; **68**: 2275–2284.
27. Dusenge ME, Madhavji S, Way DA. Contrasting acclimation responses to elevated CO2 and warming between an evergreen and a deciduous boreal conifer. *Glob Change Biol* 2020; **26**: 3639–3657.
28. Manzi OJL, Wittemann M, Dusenge ME *et al*. Canopy temperatures strongly overestimate leaf thermal safety margins of tropical trees. *New Phytol* 2024; **243**: 2115–2129.
29. Garen JC, Aparecido LMT, Blonder BW *et al*. Canopy-top measurements do not accurately quantify canopy-scale leaf thermoregulation. *Proc Natl Acad Sci USA* 2023; **120**: e2301914120.
30. Still CJ, Rastogi B, Page GFM *et al.* Imaging canopy temperature: shedding (thermal) light on ecosystem processes. *New Phytol* 2021; **230**: 1746–1753.
31. Javadian M, Smith SK, Lee K *et al.* Canopy temperature is regulated by ecosystem structural traits and captures the ecohydrologic dynamics of a semiarid mixed conifer forest site. *J Geophys Res Biogeo* 2022; **127**: e2021JG006617.
32. Jiang M, Guo K, Wang J *et al.* Current status and prospects of rice canopy temperature research. *Food Energy Secur* 2023; **12**: e424.
33. Gauthey A, Bachofen C, Deluigi J *et al.* Absence of canopy temperature variation despite stomatal adjustment in *Pinus sylvestris* under multidecadal soil moisture manipulation. *New Phytol* 2023; **240**: 127–137.
34. Mahan JR, Upchurch DR. Maintenance of constant leaf temperature by plants i. hypothesis limited homeothermy. *Environ Exp Bot* 1988; **28**: 351–357.
35. De Frenne P, Zellweger F, Rodríguez-Sánchez F *et al.* Global buffering of temperatures under forest canopies. *Nat Ecol Evol* 2019; **3**: 744–749.
36. Still CJ, Page G, Rastogi B *et al.* No evidence of canopy-scale leaf thermoregulation to cool leaves below air temperature across a range of forest ecosystems. *Proc Natl Acad Sci USA* 2022; **119**: e2205682119.
37. Crous KY, Cheesman AW, Middleby K *et al.* Similar patterns of leaf temperatures and

thermal acclimation to warming in temperate and tropical tree canopies. *Tree Physiol* 2023; **43**: 1383–1399.
38. Yi K, Smith JW, Jablonski AD *et al.* High Heterogeneity in Canopy Temperature Among Co-occurring Tree Species in a Temperate Forest. *J Geophys Res Biogeo* 2020; **125**: e2020JG005892.
39. Badgley G, Field CB, Berry JA. Canopy near-infrared reflectance and terrestrial photosynthesis. *Sci Adv* 2017; **3**: e1602244.
40. Dechant B, Ryu Y, Badgley G *et al*. NIRVP: A robust structural proxy for sun-induced chlorophyll fluorescence and photosynthesis across scales. *Remote Sens Environ* 2022; **268**: 112763.
41. Zhang, Y, Joiner J, Alemohammad SH *et al*. A global spatially contiguous solar-induced fluorescence (CSIF) dataset using neural networks. *Biogeosciences* 2018; **15**: 5779–5800.
42. Sage RF, Kubien DS. The temperature response of C_3 and C_4 photosynthesis. *Plant Cell Environ* 2007; **30**: 1086–1106.
43. Kumarathunge DP, Jiang M, Huntingford C. Potential thermal safety margin for plant photosynthesis derived from local temperature variability. *Ecol Model* 2024; **496**: 110832.
44. Luan X, Vico G. Canopy temperature and heat stress are increased by compound high air temperature and water stress and reduced by irrigation – a modeling analysis. *Hydrol Earth Syst Sci* 2021; **25**: 1411–1423.
45. Grossiord C, Buckley TN, Cernusak LA *et al.* Plant responses to rising vapor pressure deficit. *New Phytol* 2020; **226**: 1550–1566.
46. Wang J, Wen X. Increasing relative abundance of C_4 plants mitigates a dryness-stress effect on gross primary productivity along an aridity gradient in grassland ecosystems. *Plant Soil* 2022; **479**: 371–387.
47. Dusenge ME, González-Caro S, Restrepo Z *et al.* Unexpected Large Photosynthetic Thermal Plasticity of Montane Andean Trees. *Glob Change Biol* 2025; **31**: e70266.
48. Rustad L, Campbell J, Marion G *et al.* A meta-analysis of the response of soil respiration, net nitrogen mineralization, and aboveground plant growth to experimental ecosystem warming. *Oecologia* 2001; **126**: 543–562.
49. ChapinIII SF, Shaver GR, Giblin AE *et al*. Responses of arctic tundra to experimental and observed changes in climate. *Ecology* 1995; **76**: 694–711.
50. Battaglia M, Beadle C, Loughhead S. Photosynthetic temperature responses of Eucalyptus globulus and Eucalyptus nitens. *Tree Physiol* 1996; **16**: 81–89.
51. Beck HE, Zimmermann NE, McVicar TR *et al*. Present and future Köppen-Geiger climate classification maps at 1-km resolution. *Sci Data* 2018; **5**: 180214.
52. Huntingford C, Cox PM, Ritchie PDL *et al*. Acceleration of daily land temperature extremes and correlations with surface energy fluxes. *npj Clim Atmos Sci* 2024; **7**: 84.
53. IPCC. Summary for Policymakers. In: Lee H, Romero J (eds.). *Climate Change 2023: Synthesis Report. Contribution of Working Groups I, II and III to the Sixth Assessment Report of the Intergovernmental Panel on Climate Change*. Geneva: IPCC, 2023, 1–34.
54. Wang, B, Chen W, Dai J *et al.* Dryness controls temperature-optimized gross primary productivity across vegetation types. *Agr Forest Meteorol* 2022; **323**: 109073.
55. Kimball BA, Bernacchi CJ. Evapotranspiration, canopy temperature, and plant water

relations. In: Nösberger J, Long SP, Norby RJ *et al* (eds.). *Managed Ecosystems and CO2*. Berlin Heidelberg: Springer, 2006, 311–324.
56. Muller JD, Rotenberg E, Tatarinov F *et al*. Evidence for efficient nonevaporative leaf-to-air heat dissipation in a pine forest under drought conditions. *New Phytol* 2021; **232**: 2254–2266.
57. Rodrigues WP, Martins MQ, Fortunato AS *et al.* Long-term elevated air [CO_2] strengthens photosynthetic functioning and mitigates the impact of supra-optimal temperatures in tropical *Coffea arabica* and *C. canephora* species. *Glob Change Biol* 2016; **22**: 415–431.
58. Scafaro AP, Xiang S, Long BE *et al.* Strong thermal acclimation of photosynthesis in tropical and temperate wet-forest tree species: the importance of altered Rubisco content. *Glob Change Biol* 2017; **23**: 2783–2800.
59. Gottfried M, Pauli H, Futschik A *et al.* Continent-wide response of mountain vegetation to climate change. *Nat Clim Change* 2012; **2**: 111–115.
60. Fadrique B, Báez S, Duque Á *et al.* Widespread but heterogeneous responses of Andean forests to climate change. *Nature* 2018; **564**: 207–212.
61. Zellweger F, De Frenne P, Lenoir J *et al.* Forest microclimate dynamics drive plant responses to warming. *Science* 2020; **368**: 772–775.
62. Mercado LM, Medlyn BE, Huntingford C *et al*. Large sensitivity in land carbon storage due to geographical and temporal variation in the thermal response of photosynthetic capacity. *New Phytol* 2018; **218**: 1462–1477.
63. Dusenge ME, Warren JM, Reich PB *et al*. Boreal conifers maintain carbon uptake with warming despite failure to track optimal temperatures. *Nat Commun* 2023; **14**: 4667.
64. Vinod N, Slot M, McGregor IR *et al.* Thermal sensitivity across forest vertical profiles: patterns, mechanisms, and ecological implications. *New Phytol* 2023; **237**: 22–47.
65. He L, Chen JM, Gonsamo A *et al.* Changes in the shadow: The shifting role of shaded leaves in global carbon and water cycles under climate change. *Geophys Res Lett* 2018; **45**, 5052–5061.
66. Miller BD, Carter KR, Reed SC *et al*. Only sun-lit leaves of the uppermost canopy exceed both air temperature and photosynthetic thermal optima in a wet tropical forest. *Agr Forest Meteorol* 2021; **301–302**: 108347.
67. Javad A, Premugh V, Tiwari R *et al*. Leaf Temperatures in an Indian tropical forest exceed physiological limits but durations of Exposures are currently not sufficient to cause lasting damage. *Glob Change Biol* 2025; **31**: e70069.
68. Rey-Sanchez AC, Slot M, Posada JM *et al*. Spatial and seasonal variation of leaf temperature within the canopy of a tropical forest. *Clim Res* 2016; **71**: 75–89.
69. Smith B. LPJ-GUESS – an ecosystem modelling framework. https://web.nateko.lu.se/lpj-guess/guess.pdf (19 May 2026, date last accessed).
70. Dong N, Prentice IC, Harrison SP *et al*. Biophysical homoeostasis of leaf temperature: A neglected process for vegetation and land-surface modelling. *Global Ecol Biogeogr* 2017; **26**: 998–1007.
71. Bonan GB, Patton EG, Finnigan JJ *et al*. Moving beyond the incorrect but useful paradigm: reevaluating big-leaf and multilayer plant canopies to model biosphere-atmosphere fluxes – a review. *Agr Forest Meteorol* 2021; **306**: 108435.

72. Lombardozzi DL, Bonan GB, Smith NG *et al*. Temperature acclimation of photosynthesis and respiration: A key uncertainty in the carbon cycle-climate feedback. *Geophys Res Lett* 2015; **42**: 8624-8631.
73. Rogers A, Medlyn BE, Dukes JS *et al*. A roadmap for improving the representation of photosynthesis in Earth system models. *New Phytol* 2017; 213: 22–42.
74. Hulley G, Freepartner R, Malakar N *et al*. Moderate Resolution Imaging Spectrora diometer (MODIS) Land Surface Temperature and Emissivity Product (MxD21) Use r Guide. https://lpdaac.usgs.gov/documents/108/MOD21_User_Guide_V6.pdf (19 May 2026, date last accessed).
75. Islam T, Hulley GC, Malakar NK *et al.* A Physics-Based Algorithm for the Simultaneous Retrieval of Land Surface Temperature and Emissivity From VIIRS Thermal Infrared Data. *IEEE Trans Geosci Remote Sens* 2017; **55**: 563–576.
76. Didan K, Munoz AB, Solano R *et al*. MODIS Vegetation Index User's Guide (M OD13 Series). https://lpdaac.usgs.gov/documents/103/MOD13_User_Guide_V6.pdf (19 May 2026, date last accessed).
77. Doughty CE, Goulden ML. Are tropical forests near a high temperature threshold? *J Geophys Res* 2008; **113**: 2007JG000632.
78. Guo Z, Still CJ, Lee CKF *et al*. Does plant ecosystem thermoregulation occur? An extratropical assessment at different spatial and temporal scales. *New Phytol* 2023; **238**: 1004–1018.
79. Running SW, Zhao M. Daily GPP and annual NPP (MOD17A2H/A3H) and year-e nd gap- filled (MOD17A2HGF/A3HGF) products NASA earth observing system M ODIS land algorithm (for collection 6.1). https://lpdaac.usgs.gov/documents/972/MO D17_User_Guide_V61.pdf (19 May 2026, date last accessed).
80. Zhu Z, Piao S, Myneni Rb *et al*. Greening of the Earth and its drivers. *Nat Clim Change* 2016; **6**: 701–795.
81. Muñoz Sabater, J. et al. ERA5-land post-processed daily-statistics from 1950 to pre sent. https://cds.climate.copernicus.eu/datasets/derived-era5-land-daily-statistics?tab=ove rview (19 May 2026, date last accessed).
82. NOAA National Centers for Environmental Information. Global Precipitation Climat ology Project (GPCP) Climate Data Record (CDR), Version 1.3 (Daily). https://ww w.ncei.noaa.gov/access/metadata/landing-page/bin/iso?id=gov.noaa.ncdc:C00999#Docum entation (19 May 2026, date last accessed).
83. Harris I, Osborn TJ, Jones P *et al*. Version 4 of the CRU TS monthly high-resolution gridded multivariate climate dataset. *Sci Data* 2020; **7**: 109.
84. Kobayashi S, Ota Y, Harada Y *et al*. The JRA-55 reanalysis: general specifications and basic characteristics. *J Meteor Soc Japan* 2015; **93**: 5–48.

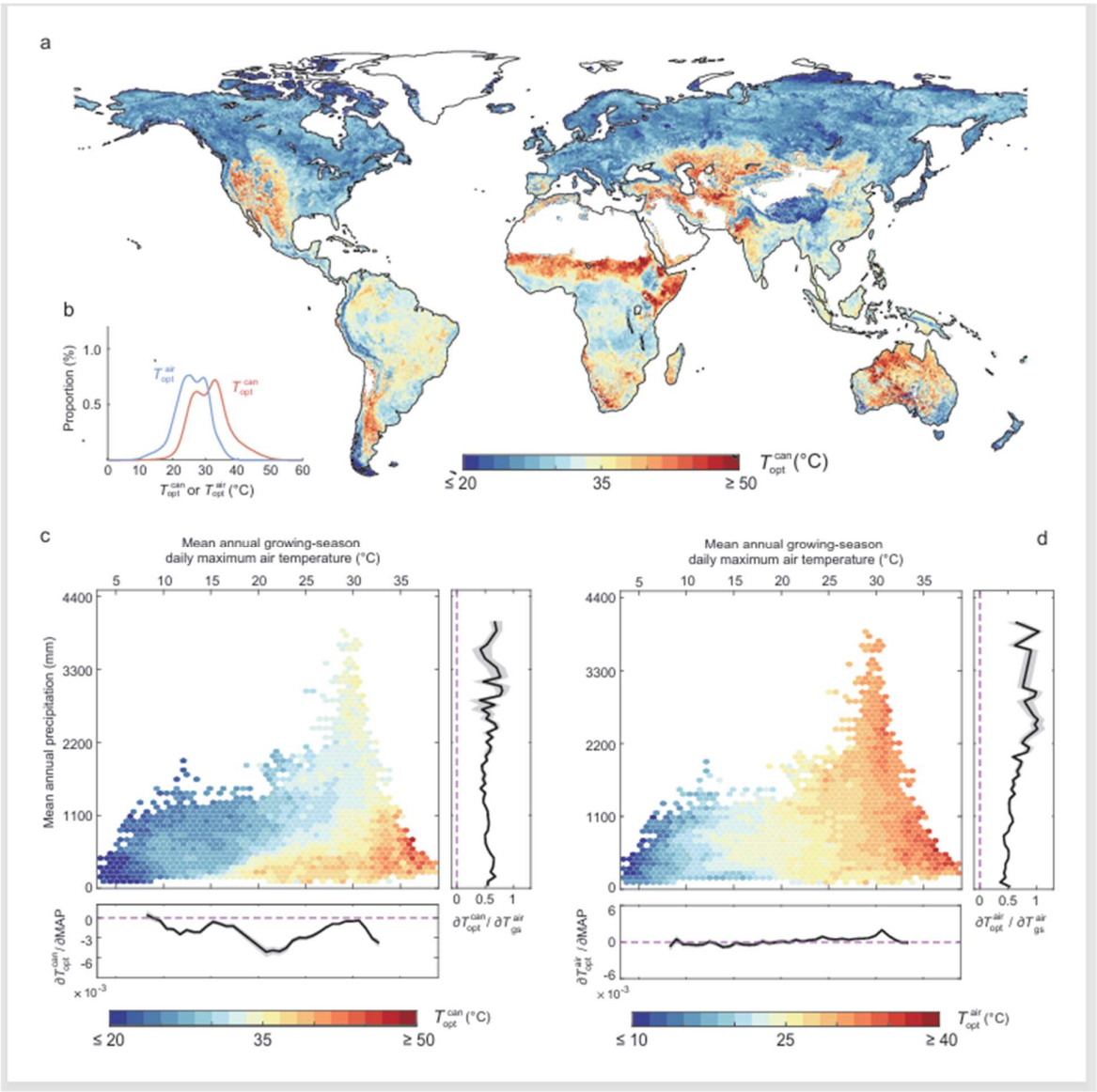

Figure 1. Distributions of derived T_{opt}^{can} and T_{opt}^{air} values for vegetation productivity and their connection to background climate. a, Spatial distribution of T_{opt}^{can} for photosynthesis determined using simultaneous canopy temperature and GPP values based on satellite observations from the Moderate Resolution Imaging Spectroradiometer (MODIS). The satellite data used covers the years 2003 to 2024 inclusive. Values are only presented for vegetated areas (i.e., for annual mean normalized difference vegetation index (NDVI) values larger than 0.1), where a value of T_{opt}^{can} is detected and where the growing season lasts longer than one month; otherwise, the location is blank (i.e., white). **b**, The red probability-density function (expressed

as a percentage), represents the distribution of T_{opt}^{can} (as shown in panel **a**) based on the proportion of its actual area relative to the total vegetated area. The blue line represents the same distribution but for T_{opt}^{air}, with the detailed spatial pattern shown in Fig. S1a. **c**, The climatic dependence of T_{opt}^{can} on air temperature and precipitation, along with relative sensitivities (side panels). Note the "*x*"-axis label and values are presented across the top of the main panels **c** and **d**. Each climatic bin was defined by intervals of 0.7℃ of mean annual growing-season daily maximum air temperature (T_{gs}^{air}) and 70-mm intervals of mean annual precipitation (MAP), based on current climatic conditions averaged between 2003 and 2024. The solid line in the extra bottom (extra right) panel represents the sensitivity to temperature (precipitation) along the precipitation (temperature) gradient, calculated as the slope of the linear regression between T_{opt}^{can} and T_{gs}^{air} (MAP) for a given level of precipitation (temperature). The shaded area indicates the standard deviation of the sensitivity ($\partial T_{opt}^{can}/\partial T_{gs}^{air}$ or $\partial T_{opt}^{can}/\partial$MAP) estimated by bootstrapping. **d,** Similar to **c**, but instead makes all calculations of T_{opt} based on air temperature rather than canopy temperature, and therefore presents variations in T_{opt}^{air}.

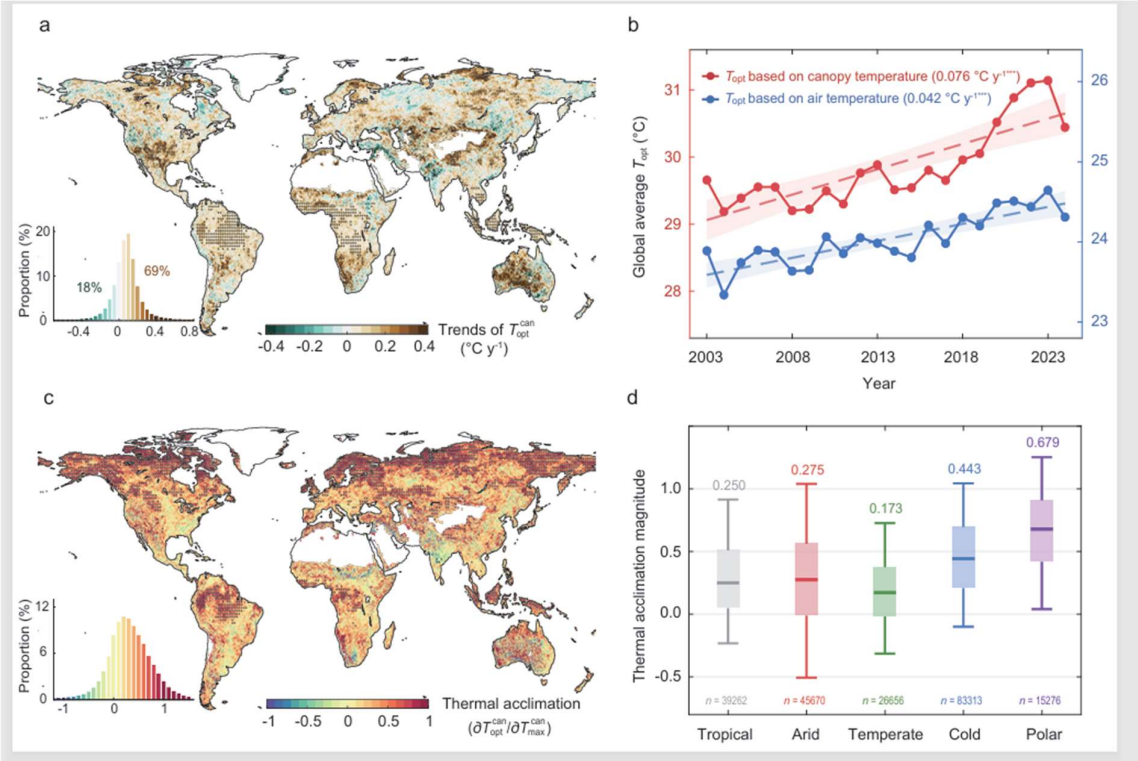

Figure 2. Temporal changes of T_{opt}^{can} and its magnitude of thermal acclimation over the last two decades. a, Spatial pattern of trends in T_{opt}^{can} from 2003 to 2024. Dot markers(·) denote grid regions where the trend is significant at the 0.05 level (P<0.05). The inset histogram shows the areal proportion across different trend magnitudes, with the total percentage annotated. **b,** The temporal changes of globally averaged T_{opt}^{can} and T_{opt}^{air} for the period 2003–2024. The solid line shows annual global means, and the dashed line represents the trend fitted using least squares regression and its 95% confidence interval as a grey plume. ***, P<0.001. **c,** Spatial distribution of the magnitude of thermal acclimation, defined as the ratio $\partial T_{opt}^{can}/\partial T_{max}^{can}$ over the last 22 years at each grid point. Regions with significant ratios (P<0.05) were marked with dot symbols. The inset histogram shows the distribution of acclimation magnitudes. **d,** difference in thermal acclimation magnitude across major climate zones. Horizontal lines denote medians, boxes represent interquartile ranges, and whiskers span the 5th–95th percentiles. Median values are displayed above each box, and sample sizes (n) are shown below. Climate zones were defined according to the 1991–2020 Köppen–Geiger climate classification [51].

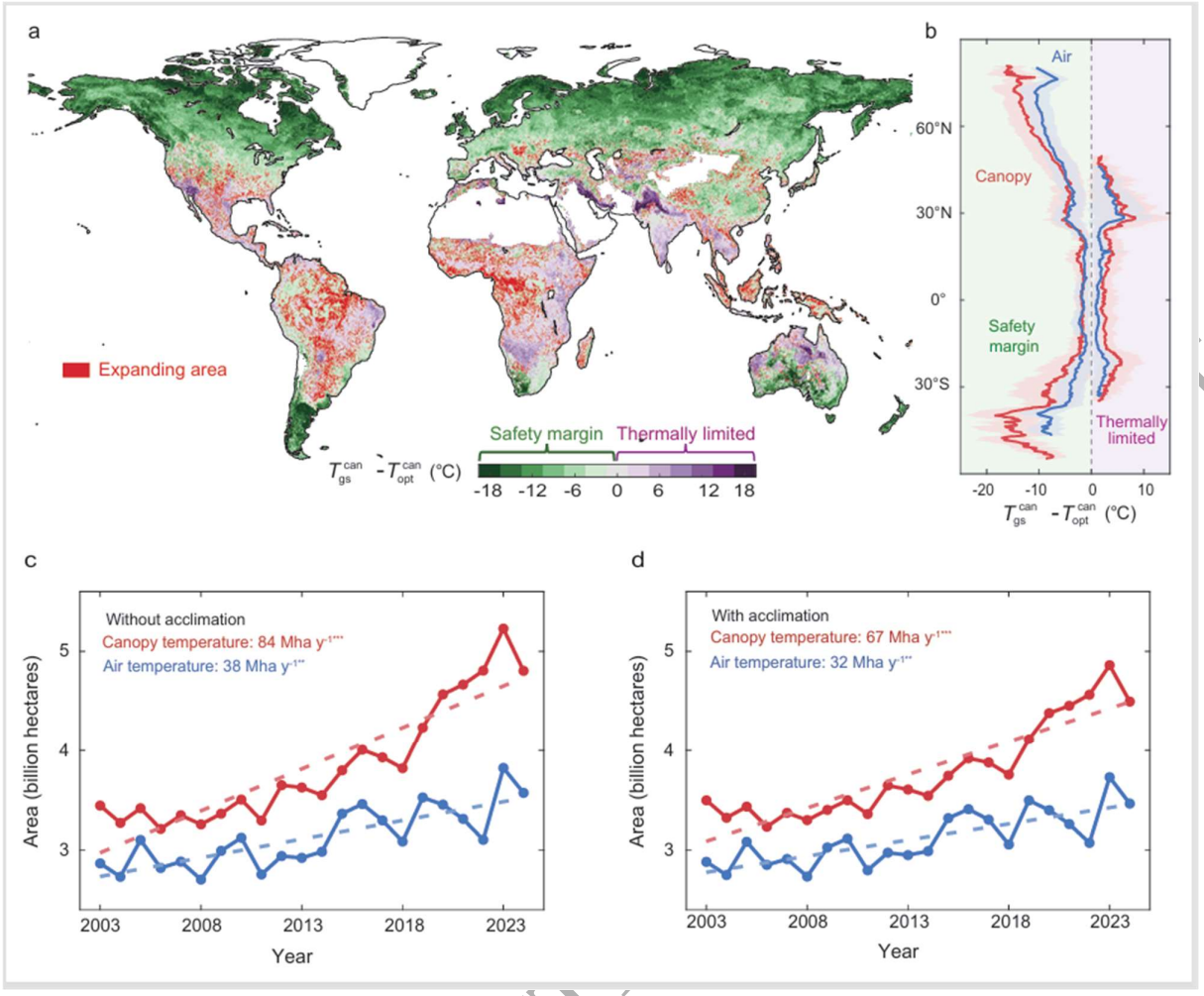

Figure 3. Patterns of the difference between T_{opt}^{can} and T_{gs}^{can}, and the expansion of thermally limited areas at canopy scale. a, The difference between the optimal canopy temperature (T_{opt}^{can}) (and so calculated similarly to the T_{opt}^{can} values in Fig. 1, and not including acclimate) and the multiyear mean growing-season average daily maximum canopy temperature (T_{gs}^{can}) during the period 2003–2024 inclusive. When T_{opt}^{can} is higher than T_{gs}^{can}, the difference represents a safety margin for vegetation productivity under warming; conversely, when T_{gs}^{can} exceeds T_{opt}^{can}, the area is already subject to thermal stress, with the difference illustrating the extent of thermal limitations on photosynthesis. This stress is due to the asymmetry of the photosynthetic response, where even a small increment in temperature above T_{opt}^{can} results in a disproportionately large suppression of productivity. The expansion of thermally limited areas without acclimation is depicted in panel **a** as a red overlay, calculated as present where T_{gs}^{can} was lower than T_{opt}^{can}

during the first five years (2003–2007) but exceeded T_{opt}^{can} in the last five years (2020–2024), corresponding to the red line in panel **c**. **b**, The latitudinal average of T_{opt}^{can} - T_{gs}^{can} based on canopy and air temperatures. Regions with safety margins and thermal limitations are calculated separately to prevent the cancellation of positive and negative values. The combined distributional pattern of T_{opt}^{air}-T_{gs}^{air} is shown in Fig. S12. **c, d,** Yearly changes over the last 22 years in the total area of thermally limited regions where the mean growing-season temperature exceeded its optimal value (i.e., where $T_{gs}^{can} > T_{opt}^{can}$). Panel **c** illustrates changes without considering thermal acclimation, and panel **d** incorporates acclimation. In panels **c** and **d**, the dashed lines represent linear-trend fits. **, $P<0.01$; ***, $P<0.001$.

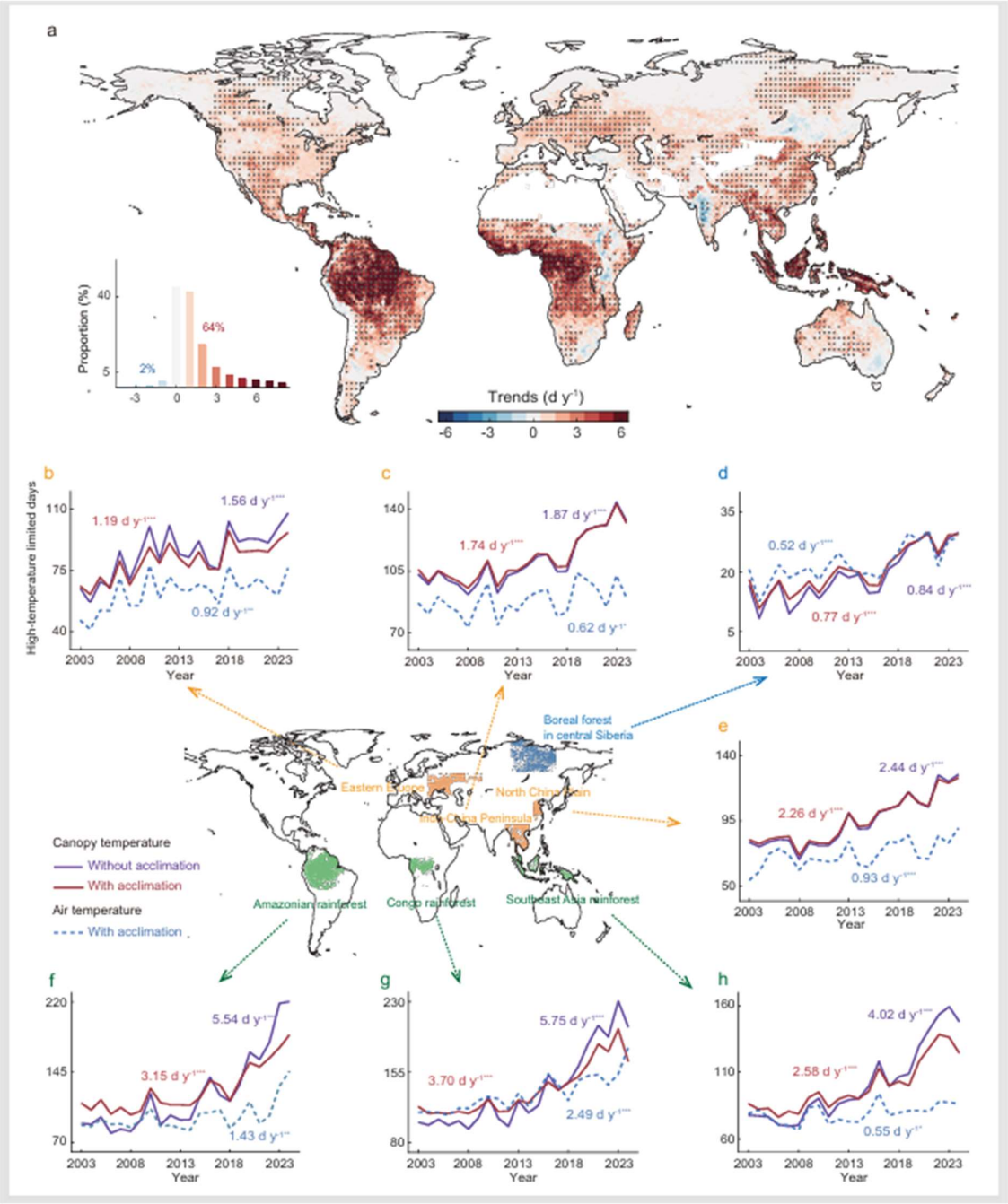

Figure 4. Trends in the number of high-temperature days over the past 22 years, with potential to suppress vegetation productivity. a, Spatial distribution of trends in the frequency of photosynthesis subjected to thermal limitation during the growing period and from years 2003 to 2024. Calculations are based on crossing derived spatially-specific values of T_{opt}^{can}, but assuming the latter are invariant in time, and thus without thermal acclimation. Trends were calculated using linear regression and the standard least squares method, and regions with

848 significant ratios (P<0.05) were marked with dot symbols. The inset histogram represents the
849 areal proportion for different trend magnitudes, binned in intervals of 1d y^{-1}. **b**–**h,** Interannual
850 variations and trends in the number of high-temperature limited days for seven key regions as
851 marked on the map: three agricultural regions (orange), including eastern Europe, Indo-China
852 Peninsula and the North China Plain, boreal forests (blue) in central Siberia, three tropical
853 rainforest regions (green) including the Amazon basin, Congo and Southeast Asia. In each panel,
854 the purple curves are calculated using canopy temperature but without allowing for acclimation
855 in T_{opt}^{can}. The red curves are identical to the purple curves, except that acclimation is incorporated
856 in T_{opt}^{can}. As a technical comparison, we also show calculations allowing for acclimation, but
857 instead forced with air temperatures, T_{opt}^{air}. Statistical significance for all text annotations are: *,
858 P<0.1; **, P<0.01; and ***, P<0.001.
859